nature communications

Article

https://doi.org/10.1038/s41467-025-62701-1

Fluctuating local polarization: a generic fingerprint for enhanced piezoelectricity in Pb-based and Pb-free perovskite ferroelectrics

Received: 31 March 2025

Accepted: 28 July 2025

Published online: 12 August 2025

Check for updates

Yonghao Yao[1], Hui Liu[1] ✉, Yihao Hu[2], Kaustuv Datta[3], Jiagang Wu[4], Yuanpeng Zhang[5], Matthew G. Tucker[5], Shi Liu[2], Joerg C. Neuefeind[5], Shujun Zhang[6] & Jun Chen[1] ✉

Understanding the atomistic mechanism underlying high piezoelectricity has long been a central focus in research of functional ferroelectric materials. Despite decades of research across various perovskite piezoelectric systems, a clear consensus on the underlying mechanisms remains elusive. We propose a new concept—fluctuating local polarization—a critical factor that effectively correlates with piezoelectricity and could serve as a generic fingerprint for enhanced piezoelectricity. This is achieved by quantitatively capturing the local polarization characteristics of 16 compositions from classical piezoelectric systems. Our findings show that greater fluctuating local polarization, considering both the magnitude and the orientation disorder of local polar displacement vectors, yields improved piezoelectric performance. High fluctuating local polarization value, corresponds to a reduced local potential energy stiffness, thereby facilitating polarization variations and resulting in an amplified piezoelectric response. The concept can further explain the performance gap between Pb-based and Pb-free ferroelectrics arising from the distinct *A*-site polar displacement characteristics. Overall, our concept offers an atomic-level insight into the enhanced piezoelectricity of perovskites and provides a theoretical framework for designing high-performance piezoelectric materials.

Ferroelectric materials, known for their capacity to interconvert electrical and mechanical energy, have found widespread applications in sensors, actuators, and ultrasound transducers. Over the past 70 years, various perovskite-type ferroelectric systems with remarkable electromechanical properties have been developed[1–5]. These systems include commercially available Pb-based materials, such as $Pb(Zr_xTi_{1-x})O_3$ (PZT)- and $Pb(Mg_{1/3}Nb_{2/3})O_3$-$PbTiO_3$ (PMN-PT)-derived systems[6], as well as Pb-free materials, such as $(K_xNa_{1-x})NbO_3$ (KNN)[7,8] - and $BaTiO_3$ (BT)- based systems[9,10]. Understanding the mechanisms underlying high piezoelectricity in these diverse materials has long been a focal

[1]Beijing Advanced Innovation Center for Materials Genome Engineering, Department of Physical Chemistry, University of Science and Technology Beijing, Beijing, China. [2]Institute of Natural Sciences, Westlake Institute for Advanced Study, Hangzhou, Zhejiang, China. [3]Helmholtz-Zentrum Berlin für Materialien und Energie, Berlin, Germany. [4]College of Materials Science and Engineering, Sichuan University, Chengdu, Sichuan, China. [5]Neutron Scattering Division, Oak Ridge National Laboratory, Oak Ridge, TN, USA. [6]Institute for Superconducting and Electronic Materials, Australian Institute of Innovative Materials, University of Wollongong, Wollongong, NSW, Australia. ✉e-mail: huiliu@ustb.edu.cn; junchen@ustb.edu.cn

point of research, as it holds the potential to shape and enhance strategies for developing new high-performance piezoelectric systems.

Over time, several theories have been proposed from different perspectives to account for the observed rise in piezoelectricity within chemically complex perovskite oxide solid solutions[10–13]. One prevailing idea is the coexistence of long-range rhombohedral (*R*), tetragonal (*T*), and/or orthorhombic (*O*) phases at the morphotropic phase boundary (MPB) or polymorphic phase boundary (PPB). The multiphase coexistence can accommodate a variety of polarization variants and thereby facilitates field-induced phase transitions or domain reorientation processes[10,14,15]. The existence of a low-symmetry monoclinic (*M*) phase, where spontaneous polarization lies within a crystallographic plane, enables easy and continuous polarization rotation under external stimulus[11,12,16–19]. Coupled with strong polarization-strain interactions, this enhances the piezoelectric response through intrinsic lattice contributions[11,12]. However, beyond these well-established intrinsic factors, other physical phenomena, such as nanodomains with a reduced coherent length of unit-cell polarizations, and the mobility of the high-density domain walls, could further enhance the piezoelectricity as extrinsic factors[20,21]. Additionally, local structural heterogeneity, represented by the polar nanoregions in relaxor ferroelectric crystals, contributes to a large shear piezoelectric response associated with the softening of the transverse acoustic mode[22,23].

While existing theories or phenomena can explain high piezoelectricity in specific systems, there is still a lack of consensus that potentially applied across Pb-based and Pb-free perovskite piezoelectric systems, such as PZT-, PMN-PT-, BT-, and KNN-based. For instance, the development of a low-symmetry phase and the corresponding argument on the enhanced piezoelectricity maybe valid for several Pb-based high-performance systems, but it cannot be applied straightaway in the cases of many Pb-free alternatives. Despite decades of research, an atomic-level understanding for high piezoelectricity that is applicable to both Pb-based and Pb-free perovskite oxide ferroelectrics is yet to be established. Moreover, the piezoelectric response of ferroelectric materials depends on the polarization variation under external stimulus[13]. Recent studies indicate that modifications of local cation environments can heavily impact the piezoelectricity even without altering the long-range average symmetry[6,23–25]. This highlights the importance of local polarization characteristics in identifying a generic phenomenon that explains elevated piezoelectricity across different perovskite oxide systems.

Herein, we elaborate a generic fingerprint of the fluctuating local polarization (P_{FL}), a quantitative descriptor of local polarization characteristics that directly correlates with the enhanced piezoelectric performance in perovskite ferroelectrics. This is achieved by capturing the characteristics of local polar displacement vectors (***D***) in 16 compositions, covering both Pb-based and Pb-free piezoelectric systems. The P_{FL}-driven piezoelectricity can further explain the performance gap between Pb-based and Pb-free systems, stemming from the larger polar displacement of *A*-site cations in Pb-based materials compared to those in Pb-free systems.

Results and discussion

Quantitative description of local polarization state

High-performance piezoelectric materials are typically chemically complex solid solutions, where multiple cations occupy equivalent crystallographic sites. Differences in the ionic polarizability, atomic radius, or valence states of these cations cause them to deviate away from their crystallographic positions, manifesting as disorder that disrupts the average polarization that is constrained by the long-range structural symmetry. Considering the weak polarization anisotropy typically associated with the diverse local polarization variants in a system, the disorder of local polar displacements induced by the chemical complexity would impact the piezoelectricity. The study of atomic pair-distribution function (PDF), calculated from the total scattering function, incorporates both the Bragg diffraction and diffuse scattering[26–28], therefore allows for study of local and nanoscale structures that go beyond the long-range symmetry of crystalline materials[29,30].

To characterize the features of the local polarization disorder, we employed advanced neutron total scattering experiment combined with RMC modelling[31–33]. The steps are illustrated in Fig. 1, taking the relatively high-performance Pb-free piezoelectric $K_{0.48}Na_{0.52}Nb_{0.955}Sb_{0.045}O_3$ (KNNS) as an example. The starting supercells were constructed based

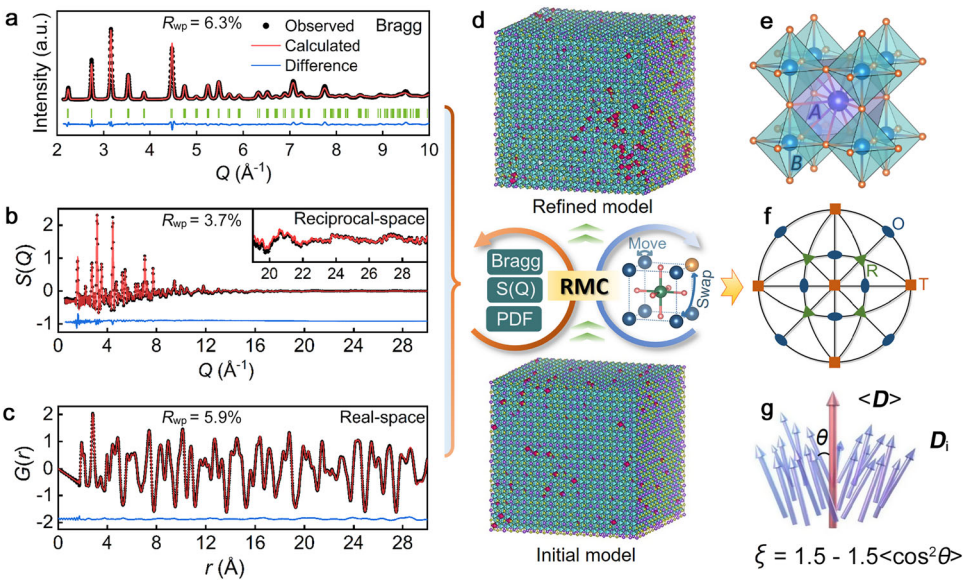

Fig. 1 | The workflow schematic of extracting local polarization characteristics based on the neutron total scattering and RMC modelling. a–d Bragg, reciprocal-space *S*(*Q*), and real-space *G*(*r*) data simultaneously fitted by RMC algorithm to get the refined 3D atomic configurations for KNNS. The black dots, red lines, and blue lines represent the observed data, the fitted calculated data, and the difference curve, respectively. **e** The local oxygen environment of *A*-site and *B*-site cations in a perovskite-type structure. **f** Stereographic projection along the $[001]_c$ direction and (**g**), the orientation disorder parameter of local polar displacement vectors (***D***). The <***D***> indicates the average vector, while the θ represents the deviation of $\boldsymbol{D}_i$ from the direction of <***D***>.

https://doi.org/10.1038/s41467-025-62701-1

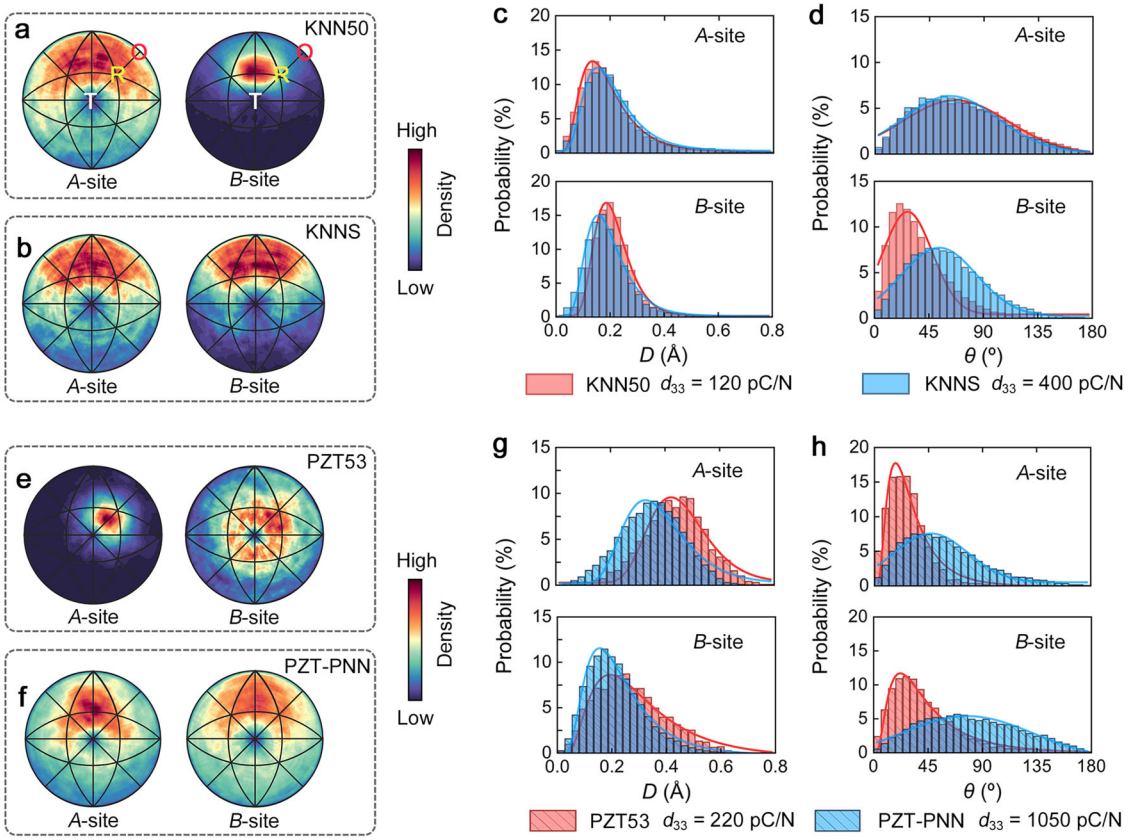

Fig. 2 | Characteristics of *A*/*B*-site polar displacement vectors in two KNN-based and two PZT-based systems. a, **b**, **e**, **f** The stereographic projection of local polar displacement vector with respect to $[001]_c$. The right color bars represent the density of polar displacement vectors. **c**, **g** the magnitude and **d**, **h** the angle histograms of local polar displacement vectors. θ indicates the angle of each displacement vector away from the direction of average polar displacement vector $<\boldsymbol{D}>$.

on the average crystal structure derived from the Rietveld refinements of the neutron powder diffraction data. During the RMC modelling process, the atoms undergo random iterative movements and position-swaps to fit multiple experimental datasets, including the neutron Bragg data, the real-space data $G(r)$, and the reciprocal-space data $S(Q)$ (Fig. 1a–d). From the refined atomic configurations, the local polarization states, represented by the local polar displacement vectors ($\boldsymbol{D}$), can be directly calculated as the off-centering displacement vector in the AO_{12} and BO_6 cages (Fig. 1e). Unlike the single specific $\boldsymbol{D}$ obtained from the average structure refinement, this method provides a more comprehensive description of $\boldsymbol{D}$ by providing a distribution. Additionally, we focus on the orientation and magnitude of $\boldsymbol{D}$ to explore the characteristics of local spontaneous polarization across different piezoelectric systems.

We have extracted the degree of orientation disorder and the mean magnitude of $\boldsymbol{D}$ ($<D>$) to quantify the characteristics of the local polarization state. The orientation order parameter S, often used to describe nematic ordering in liquid crystals[34], is calculated as $1.5 < \cos^2\theta > -0.5$[33,35], where θ represents the angle of each displacement vector away from the direction of average polar displacement vector ($<\boldsymbol{D}>$), the notation $< >$ indicates averaging (Fig. 1g). A detailed definition of S is provided in the supplementary information. However, according to the definition of S, it should be noted that this order parameter is suitable for ferroelectric-based systems but may not be applicable to paraelectric, antiferroelectric, or fully disordered relaxor systems. The disorder parameter ξ is defined as $1 - S$ to quantify the degree of disorder in the orientation of the $\boldsymbol{D}$[33]. $\xi = 0$ signifies perfect ordering, indicating that all polar displacement vectors are along the same direction in the ferroelectric-based systems, while $\xi \sim 1$ represents high directional disorder of these vectors. To validate the accuracy of our modelling, the polarization feature of $PbTiO_3$ (PT) were calculated. The obtained mean magnitude polarization value is 55 μC/cm² with a disorder parameter ξ of 0.03 (Supplementary Fig. 1), which are in good agreement with previously reported results[35,36]. Therefore, a combined evaluation of the magnitudes as well the orientation disorder of $\boldsymbol{D}$ can be provided to describe deeply the local polarization state in a ferroelectric system.

Configuration of local polar displacement vectors

Two chemically modified Pb-free KNN-based materials, namely $(K_{0.5}Na_{0.5})NbO_3$ (KNN50) and its modified variant KNNS, as well as the classical PZT-based composition of $PbZr_{0.53}Ti_{0.47}O_3$ (PZT53) and its chemical modified counterpart $0.135PbZrO_3$-$0.315PbTiO_3$-$0.55Pb(Ni_{1/3}Nb_{2/3})O_3$ (PZT-PNN), were investigated first to explore the relationship between the piezoelectric performance and the local polar displacement vectors. Specifically, KNN50 exhibits inferior piezoelectricity (d_{33} = 120 pC/N), while KNNS displays relatively high piezoelectricity (d_{33} = 400 pC/N). Similarity, the PZT53 demonstrates inferior piezoelectricity (d_{33} = 220 pC/N), whereas PZT-PNN exhibits ultrahigh piezoelectricity (d_{33} = 1050 pC/N).

The configurations of A-site polar displacement vector ($\boldsymbol{D}_A$) and B-site polar displacement vector ($\boldsymbol{D}_B$) were extracted from the refined atomic configurations (Fig. 2), following the procedure outlined in Fig. 1. The left panel displays stereographs depicting the directional disorder, while the right panel presents histograms of the displacement magnitudes and their angular deviations relative to the average vector. Evidently, for the KNN-based system, the $\boldsymbol{D}_B$-distribution of KNN50 demonstrates a statistical preference along $[011]_c$ with a

https://doi.org/10.1038/s41467-025-62701-1

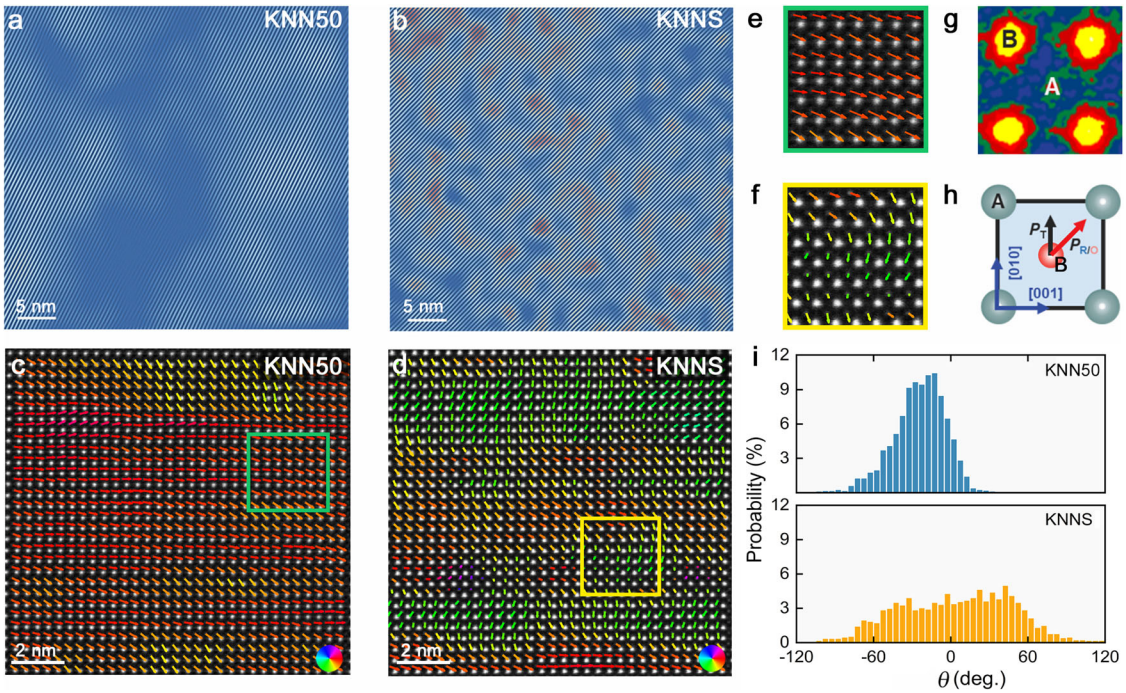

Fig. 3 | Distributions of local polarization states revealed by the high-resolution STEM of KNN-based piezoelectric system. a, **b** The IFFT images obtained by masking the (110) spots in HRTEM images. **c**, **d** the STEM-HADDF images recorded along the $[001]_c$ zone axis along with the *A*-site displacement vectors mapping. **e**, **f** representative enlarged images from (**c** and **d**), respectively. **g**, **h** the schematic of displacement vector calculation. **i** angle histograms of the *A*-site and *B*-site displacement vectors. The angle of 0° indicates the $[110]_c$ direction.

moderate level of angular deviations (Fig. 2a), while the $\boldsymbol{D}_B$-directions in KNNS exhibit a much broader range of deviations covering a larger area of the stereograph (Fig. 2b). On the other hand, the distributions of $\boldsymbol{D}_A$ remain notably similar in both compositions. These observed direction-distributions of $\boldsymbol{D}_B$ are consistent with the reported long-range orthorhombic phase in KNN50[37] and align with the concept of multi-phase coexistence in KNNS[24,38]. Statistical analysis of the polar displacement vectors indicates a minor difference of $\boldsymbol{D}_A$, not only from the magnitude, but also from the angular distribution. Interestingly, there is a significant diffusion of θ for the $\boldsymbol{D}_B$ in KNNS compared to KNN50 (Fig. 2d). This suggests an increased disorder of $\boldsymbol{D}_B$ may lead to enhanced piezoelectricity in Pb-free systems.

For PZT-based system, the directions of both $\boldsymbol{D}_A$ and $\boldsymbol{D}_B$ display a much more dispersed distribution in the high-performance PZT-PNN compared to inferior performance PZT53, while the magnitude changes mildly (Fig. 2e–h). This suggests that a broader direction distribution of $\boldsymbol{D}$ generally leads to elevated piezoelectricity in both Pb-free and Pb-based systems. Interestingly, these two PZT-based compositions possess a large mean magnitude of $\boldsymbol{D}_A$ (0.35 Å in PZT-PNN, 0.44 Å in PZT53) compared to the two KNN-based compositions (both about 0.2 Å), while there is not much difference in the mean magnitude of $\boldsymbol{D}_B$ (about 0.21 Å). As the magnitudes of $\boldsymbol{D}_B$ remain comparable among those systems, it is highly indicative that the performance gap between the Pb-free and Pb-based materials may exclusively originate from the distinct behaviour of the *A*-site cations.

The atomic resolution scanning transmission electron microscopy (STEM) technique was further employed to complement the observations from RMC method, with KNN50 and KNNS serving as examples (Fig. 3). KNNS, with its relatively high piezoelectricity, exhibits a wider variation of local distortions compared to KNN50, as revealed by the inverse Fast Fourier Transform (IFFT) of HRTEM (Fig. 3a, b and Supplementary Fig. 2a, b). The 2D atomic displacement mapping is extracted from the high-angle annual dark field (HAADF)-STEM, based on the position of *A*/*B*-site atomic columns (Fig. 3c–h and Supplementary Fig. 2c, d). In KNN50, predominant displacement occurs along the $[011]_c$, with small fluctuations, resulting in a consistent color distribution within a 5-10 nm range. In contrast, KNNS displays smaller clusters of displacement vectors. Statistically, over 8000 displacement vectors were analyzed to confirm the distribution of displacement vector angles. The results clearly illustrate a broader angle distribution in KNNS compared with KNN50, confirming the observation in Fig. 2a–d. Such a continuous and broad distribution of polar displacement vectors, observed in other ferroelectric materials with high piezoelectricity, can therefore be considered to facilitate polarization rotation and thus enhancing piezoelectricity[39,40]. This observation again suggests that higher disorder in local polar displacement vectors favors higher piezoelectricity.

Fluctuating local polarization and piezoelectricity

The above results suggest clearly that the macroscopic piezoelectric response is highly correlated with the local polarization configuration, and a ferroelectric system with higher piezoelectricity possesses a more disordered local polarization state. To gain a deeper understanding of how local polarization configuration influence piezoelectricity, we studied several prominent perovskite-type Pb-based and Pb-free piezoelectrics with varying piezoelectric coefficient d_{33}. The detailed compositions are listed in Supplementary Table 1, with Pb-based systems exhibiting piezoelectric coefficients ranging from 80 to 1050 pC/N, and Pb-free systems showing values between 120 and 600 pC/N. The respective RMC fitting results for each composition are provided in Supplementary Fig. 3. The R_{wp} values of the RMC fitting results (Supplementary Table 2) for all systems indicate that the data were well-fitted simultaneously. Note that the extracted stereographic projections of local polar displacement vectors of PZT45, PZT53, PT, BT, and BCZT (Supplementary Fig. 4) agree well with previous studies[29,31,35,41].

The critical parameters, including the disorder parameter ξ and the mean magnitude of $\boldsymbol{D}$ (<*D*>), both for *A*-site and *B*-site polar displacements in various piezoelectric systems, were extracted and presented in Fig. 4a, b. Two distinct subgroups are observed for Pb-based

https://doi.org/10.1038/s41467-025-62701-1

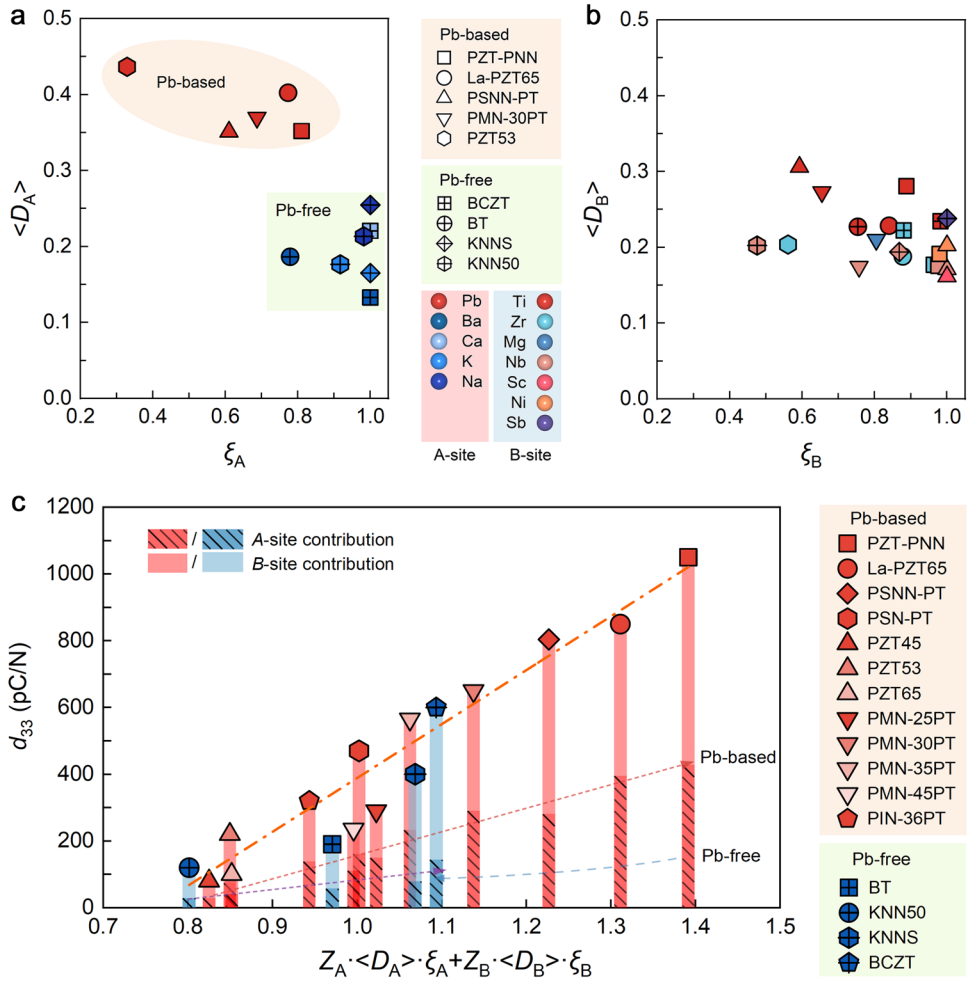

Fig. 4 | Strong correlation between fluctuating local polarization and piezoelectricity in various piezoelectric systems. a, **b** the plots of disorder parameter ξ and the mean magnitude <*D*> of *A*-site and *B*-site local polar displacement vectors, respectively. Different colors correspond to different atoms, while different shapes represent various systems. **c** the piezoelectric coefficient d_{33} as a function of fluctuating local polarization P_{FL}, defined as Z_A·<D_A>·ξ_A + Z_B·<D_B>·ξ_B. The red bars represent Pb-based systems, and the blue bars represent Pb-free systems.

and Pb-free systems in the plot of ξ *vs.* <*D*> of the *A*-site, while no significant difference exists in the case of *B*-site cations. A common characteristic of a high ξ_A value close to 1 occurs in the Pb-free systems, which is notably higher than that in Pb-based systems. While the mean magnitude <D_A> in the Pb-free systems is considerably lower than Pb-based systems. For example, both the Ba^{2+} and Ca^{2+} have a large ξ value of near 1 in the relatively high-performance BCZT (d_{33} = 600 pC/N), which is higher than the ξ_A value of 0.77 in the ultrahigh-performance PZT-PNN (d_{33} = 1050 pC/N). Despite this, PZT-PNN has a larger <D_A> of Pb^{2+} of 0.35 Å compared to 0.22 Å for Ca^{2+}, and 0.13 Å for Ba^{2+} in BCZT. Note that these compositions with high piezoelectricity, whether Pb-based or Pb-free, typically have a relatively high ξ value. For example, La-PZT65 and PZT-PNN have ξ values above 0.7, while KNNS and BCZT have ξ values above 0.8 for both the *A*-site and *B*-site. This scenario is also observed in individual solid solutions, such as the PZT and PMN-PT systems with varying Ti content, where MPB compositions exhibit higher ξ values as compared to the non-MPB compositions. Interestingly, although the Pb-free systems present high ξ_A, and similar values of ξ_B and <D_B>, their piezoelectric d_{33} is still lower than that of the Pb-based systems. This indicates that piezoelectricity is governed not only by the orientational disorder of local polarization vectors but also by their magnitude.

To integrate these two critical parameters, disorder parameter and the magnitude of $\boldsymbol{D}$, we introduced a new parameter called fluctuating local polarization (P_{FL}), which is defined as $P_{FL} = \Sigma_i Z_i \cdot \langle D_i \rangle \cdot \xi_i$, where Z_i represents the charge of the different cations, and the nominal charge was utilized to simplify the calculation. The P_{FL} reflects the accumulated states of electric dipole moments (Z·<D>) from both *A*-site and *B*-site. In other words, P_{FL} effectively captures the directional distribution and the magnitude of *A*/*B*-site electric dipole moments. A larger value of P_{FL} requires not only a large magnitude but also high disorder characteristics of *A*/*B*-site electric dipole moments. Interestingly, the plot of d_{33} as a function of P_{FL} reveals a compelling correlation in both Pb-based and Pb-free systems (Fig. 4c). The piezoelectric d_{33} demonstrates a strong positive correlation with the P_{FL} value, where a larger P_{FL} value corresponds to a higher d_{33}. For example, the considerable enhancement in disorder of both $\boldsymbol{D}_A$ and $\boldsymbol{D}_B$ from PZT65 to La-PZT65, leads to a P_{FL} value increases from 0.85 to 1.31, and corresponding to a d_{33} enhancement from 100 to 850 pC/N. Similarly, the rise in ξ_B from KNN50 to KNNS, results in a P_{FL} value increase from 0.8 to 1.07, leading to a d_{33} increase from 120 to 400 pC/N.

Notably, despite BCZT exhibits very high ξ ~ 1 values for both *A*-site and *B*-site, its relatively low <D_A> value results in a moderate P_{FL} value of 1.1, yielding a relatively high d_{33} of 600 pC/N. This highlights that enhancing piezoelectricity requires not just the orientation disorder of local polar displacement vectors, but also maintaining a significant magnitude. From thermodynamic theory, the critical role of high P_{FL} stems from the interplay between significant orientational

disorder—reducing polarization anisotropy—and large local polarization magnitudes, which collectively contribute to a flattened free-energy landscape across a broad polarization range. These features enable larger polarization variations under small external fields, enhance polarization-lattice coupling, and ultimately lead to a heightened piezoelectric response.

Piezoelectric performance gap between Pb-based and Pb-free materials

Based on the quantifiable relationship between P_{FL} and d_{33}, the individual piezoelectric contributions from the *A*-site and *B*-site can be evaluated. The piezoelectric contribution from *A*-site in the Pb-free systems (dark blue shaded columns, typically below 30%) is much smaller than that in Pb-based systems (dark red shaded column, typically 45%), owing to the lower values of $\langle D_A \rangle$ (Fig. 4c and Supplementary Fig. 5). The observed piezoelectricity gap in Pb-based and Pb-free systems can be attributed to the distinct behaviour of *A*-site polar displacement, wherein Pb-free systems exhibit smaller magnitude of *A*-site local polar displacement compared to Pb-based systems. For example, the piezoelectric contribution from *B*-site ($Z_B \cdot \langle D_B \rangle \cdot \xi_B$) is similar for BCZT ($d_{33}$ = 600 pC/N) and La-PZT65 (d_{33} = 850 pC/N). However, BCZT has a lower value of $Z_A \cdot \langle D_A \rangle \cdot \xi_A$ compared to La-PZT65 despite having a higher value of ξ_A (Supplementary Fig. 5). Importantly, in Pb-free systems, it appears challenging to largely increase the P_{FL} from the *A*-site by enhancing the disorder (Fig. 4a), due to the inherently high disordering. In these systems, the piezoelectric enhancement through chemical modifications mainly arising from *B*-site disordering (Supplementary Fig. 6). In contrast, Pb-based systems still have considerable potential to improve disorder, as both the *A*-site and *B*-site can accommodate large polar displacement. This atomic-level observation aligns with the greater ease of achieving a d_{33} value of 1000 pC/N in Pb-based ceramics[3], while Pb-free KNN-based and BT-based ceramics are typically limited to below 700 pC/N[8]. The different behaviour of *A*-site atoms in Pb-based and Pb-free systems thus provides a key insight into why Pb-free piezoelectric systems generally exhibit inferior performance compared to Pb-based systems.

DFT calculations and *A*-site susceptibility

To further explore the atomic-level mechanisms underlying the relationship between P_{FL} and piezoelectricity, density functional theory (DFT) calculations were employed. DFT calculations were performed on relatively simple systems with representative compositions, including Pb-based PZT65 and La-PZT65, as well as Pb-free KNN50 and KNNS. A broadened D_B distribution from DFT calculations is observed in high piezoelectric performance compositions such as La-PZT65 (d_{33} = 850 pC/N) and KNNS (d_{33} = 400 pC/N), compared with their lower-performing counterparts, PZT65 (d_{33} = 120 pC/N) and KNN50 (d_{33} = 120 pC/N) (Supplementary Fig. 7c). This observation is consistent with the results obtained from RMC fitting and STEM analysis.

To understand the role of local polarization in piezoelectricity, we examined the sensitivity of local potential energy ($\langle k \rangle$) of each *A*-site ions, which measures the position shift from small perturbation[40]. A smaller value of $\langle k \rangle$ corresponds to the larger ions shift under a small external field, thus reflecting a higher piezoelectric response. Significantly, the higher value of P_{FL} also suggests easier ions shifting, analogous to the smaller $\langle k \rangle$. As depicted in Fig. 5, an increase in the P_{FL} from PZT65 to La-PZT65, as well as from KNN50 to KNNS, corresponds to a decrease in the $\langle k \rangle$ value, consequently resulting in a significant enhancement in the piezoelectric response.

Interestingly, a pronounced difference in the $\langle k \rangle$ values between Pb-based and Pb-free systems is observed, with the $\langle k \rangle$ values of the PZT65-based compositions being considerably lower than those of the KNN-based compositions. This coincides with the performance gap elucidated in Pb-based and Pb-free system. Notably, the $\langle k \rangle$ value of La-PZT65 is smaller than that of KNNS, corresponding to its higher

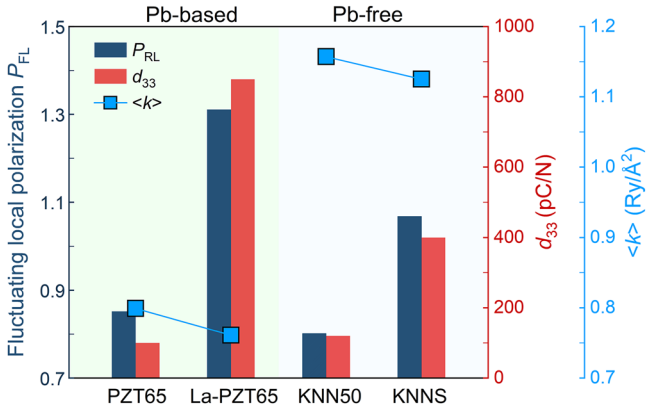

Fig. 5 | Correlation between d_{33} and the susceptibility ($\langle k \rangle$) from DFT calculation.

piezoelectric performance. The different $\langle k \rangle$ values for *A*-site atoms in Pb-based and Pb-free systems contribute to the understanding of the piezoelectricity gap. The weak coupling between *A*-site atoms and oxygen in Pb-free systems (Supplementary Fig. 7b) contrasts with the strong *A-O* hybridization in Pb-based systems[42] (Supplementary Fig. 7a) due to the lone pair of Pb^{2+}, accounting for a smaller value of $\langle k \rangle$ observed in Pb-based systems. These features suggest lower local potential energy stiffness and stronger polarization-lattice coupling in Pb-based systems, which contribute to their superior piezoelectric performance.

The high value of P_{FL} indicates a larger variety of polarization states, signifying a broader spatial configuration of polar displacement available for polarization variation. The orientation disorder in polar displacements corresponds to the reduced polarization anisotropy, accompanied with large magnitude of polar displacements, corresponds to a flattened energy landscape over wide polarization length range. This feature leads to a large effective polarization variation and enhances polarization-lattice coupling with external stimulus, and resulting heightened piezoelectricity. Notably, this diversity in polar displacement is reflected in the polarization within the unit cell, leading to the presence of multiple polarization orientations in perovskite ferroelectric materials. Established piezoelectric mechanisms, such as multi-phase coexistence, local heterogeneity, and low-symmetry phase, also emphasize the role of increased polarization orientation diversity. For example, the phase coexistence at MPBs or PPBs correlates with diverse polarization variants from different phases. These phenomena are linked to the reduction of polarization anisotropy, correspond to a low energy barrier for polarization reorientation under external fields, and ultimately leading to enhanced piezoelectric performance[1,4,8,43].

From a materials design perspective, achieving a high value of P_{FL} is crucial for attaining high piezoelectricity. This study suggests chemical composition design principles for both high-performance Pb-based and Pb-free systems. It is important to maintain a large $\langle D \rangle$ when introducing high disorder ξ. The prime examples include our recently reported high piezoelectricity in high-entropy compositions, such as PNN-PIN-PT (d_{33} = 920 pC/N), PNN-PSN-PT (d_{33} = 804 pC/N)[40], and the designed PNN-PIN-PZT (d_{33} = 1010 pC/N) (Supplementary Fig. 8). In these examples, since the Pb atoms effectively maintain large *A*-site polar displacement, the improvement in piezoelectric performance is primarily achieved by introducing disorder through chemical substitution. Conversely, in Pb-free systems, the low $\langle D_A \rangle$ (such as Ba^{2+}, Ca^{2+}, Sr^{2+}, K^+, Na^+) limits the performance enhancement, even though a high degree of disorder can be achieved. The $6s^2$ lone pair electron is crucial for the high $\langle D_A \rangle$ in Pb-based systems. Looking at the periodic table, the Bi^{3+} and Tl^+ possess a similar lone pair configuration to Pb^{2+}. However, the small ionic radius of Bi^{3+} results in

long-range oxygen octahedron tilting[44], typically leading to a high local polar displacement ordering that hinders the piezoelectric performance enhancement. Additionally, Tl^+ is a highly toxic element. Therefore, Pb-free materials are unlikely to achieve the same high level of d_{33} as Pb-based materials solely through chemical compositional design. Overall, the concept of P_{FL} can provide a theoretical framework for designing high-performance Pb-based piezoelectric materials, and offers insight into the difficulties in developing high-performance Pb-free materials.

In summary, we have introduced a phenomenological model—called fluctuating local polarization—as a quantitative measure to describe the atomic-level polar displacement characteristics, demonstrating a strong correlation with the observed piezoelectricity in both Pb-based and Pb-free systems. The model considers both the magnitudes and disorder of local polarization vectors, which ultimately influence the local potential energy surfaces and determine the adaptability of inherent polarizations under external stimuli. This quantitative measure, derived from nanoscale structural information, not only explains the development of piezoelectric activity within specific systems and the distinct macroscopic properties of Pb-based and Pb-free materials, but also complements existing theories, such as the role of low-symmetry monoclinic phases in Pb-based materials, in describing enhanced piezoelectric activity as a function of composition. As such, the proposed concept offers a potential fingerprint for understanding the evolving local structural correlations that drive extraordinary piezoelectricity in both Pb-based and Pb-free systems. It provides a theoretical foundation for designing high-performance perovskite piezoelectric materials. Furthermore, this simple concept could be extended beyond ferroelectric systems, making it applicable to other ordered/disordered functional materials, including those exhibiting magnetic and/or charge-ordering phenomena.

Methods

The detailed sample preparation and structural characterization methods are provided in the Supplementary Information file.

Data availability

Relevant data supporting the key findings of this study are available within the paper and the supplementary information file. The data generated in this study are provided in the Source Data file. Source data are provided with this paper.

References

1. Jaffe, B., Cook, W. R. Jr & Jaffe, H. *Piezoelectric Ceramics* (Academic Press, 1971).
2. Rödel, J. et al. Perspective on the development of lead design of lead-free piezoceramics. *J. Am. Ceram. Soc.* **92**, 1153–1177 (2009).
3. Zhang, S. et al. Advantages and challenges of relaxor-$PbTiO_3$ ferroelectric crystals for electroacoustic transducers – a review. *Prog. Mater. Sci.* **68**, 1–66 (2015).
4. Li, J.-F., Wang, K., Zhu, F.-Y., Cheng, L.-Q. & Yao, F.-Z. (K, Na)NbO_3-based lead-free piezoceramics: fundamental aspects, processing technologies, and remaining challenges. *J. Am. Ceram. Soc.* **96**, 3677–3696 (2013).
5. Sun, E. & Cao, W. Relaxor-based ferroelectric single crystals: growth, domain engineering, characterization and applications. *Prog. Mater. Sci.* **65**, 124–210 (2014).
6. Li, F. et al. Giant piezoelectricity of Sm-doped $Pb(Mg_{1/3}Nb_{2/3})O_3$-$PbTiO_3$ single crystals. *Science* **364**, 264–268 (2019).
7. Saito, Y. et al. Lead-free piezoceramics. *Nature* **432**, 84–87 (2004).
8. Lv, X., Zhu, J., Xiao, D., Zhang, X. -x & Wu, J. Emerging new phase boundary in potassium sodium-niobate based ceramics. *Chem. Soc. Rev.* **49**, 671–707 (2020).
9. Liu, W. & Ren, X. Large piezoelectric effect in Pb-free ceramics. *Phys. Rev. Lett.* **103**, 257602 (2009).
10. Acosta, M., Novak, N., Jo, W. & Rödel, J. Relationship between electromechanical properties and phase diagram in the $Ba(Zr_{0.2}Ti_{0.8})O_3$–$x(Ba_{0.7}Ca_{0.3})TiO_3$ lead-free piezoceramic. *Acta Mater.* **80**, 48–55 (2014).
11. Noheda, B. et al. Stability of the monoclinic phase in the ferroelectric perovskite $PbZr_{1-x}Ti_xO_3$. *Phys. Rev. B* **63**, 014103 (2000).
12. Fu, H. & Cohen, R. E. Polarization rotation mechanism for ultrahigh electromechanical response in single-crystal piezoelectrics. *Nature* **403**, 281–283 (2000).
13. Damjanovic, D. Contributions to the piezoelectric effect in ferroelectric single crystals and ceramics. *J. Am. Ceram. Soc.* **88**, 2663–2676 (2005).
14. Liu, H. et al. Role of reversible phase transformation for strong piezoelectric performance at the morphotropic phase boundary. *Phys. Rev. Lett.* **120**, 055501 (2018).
15. Zhang, M.-H. et al. Deciphering the phase transition-induced ultrahigh piezoresponse in (K,Na)NbO_3-based piezoceramics. *Nat. Commun.* **13**, 3434 (2022).
16. Viehland, D. Symmetry-adaptive ferroelectric mesostates in oriented $Pb(BI_{1/3}BII_{2/3})O_3$-$PbTiO_3$ crystals. *J. Appl. Phys.* **88**, 4794–4806 (2000).
17. Noheda, B. et al. Polarization rotation via a monoclinic phase in the piezoelectric 92% $PbZn_{1/3}Nb_{2/3}O_3$-8% $PbTiO_3$. *Phys. Rev. Lett.* **86**, 3891–3894 (2001).
18. Damjanovic, D. A morphotropic phase boundary system based on polarization rotation and polarization extension. *Appl. Phys. Lett.* **97**, 062906 (2010).
19. Liu, H. et al. Critical role of monoclinic polarization rotation in high-performance perovskite piezoelectric materials. *Phys. Rev. Lett.* **119**, 017601 (2017).
20. Theissmann, R. et al. Nanodomains in morphotropic lead zirconate titanate ceramics: on the origin of the strong piezoelectric effect. *J. Appl. Phys.* **102**, 024111 (2007).
21. Jin, Y. M., Wang, Y. U., Khachaturyan, A. G., Li, J. F. & Viehland, D. Conformal miniaturization of domains with low domain-wall energy: monoclinic ferroelectric states near the morphotropic phase boundaries. *Phys. Rev. Lett.* **91**, 197601 (2003).
22. Li, F. et al. The origin of ultrahigh piezoelectricity in relaxor-ferroelectric solid solution crystals. *Nat. Commun.* **7**, 13807 (2016).
23. Li, F. et al. Ultrahigh piezoelectricity in ferroelectric ceramics by design. *Nat. Mater.* **17**, 349–354 (2018).
24. Gao, X. et al. The mechanism for the enhanced piezoelectricity in multi-elements doped (K,Na)NbO_3 ceramics. *Nat. Commun.* **12**, 881 (2021).
25. Zou, J. et al. Enhancing piezoelectric coefficient and thermal stability in lead-free piezoceramics: insights at the atomic-scale. *Nat. Commun.* **15**, 8591 (2024).
26. Keen, D. A. Total scattering and the pair distribution function in crystallography. *Crystallogr. Rev.* **26**, 143–201 (2020).
27. Egami, T. & Billinge, S. J. L. *Underneath the Bragg Peaks: Structural Analysis of Complex Materials* (Oxford University Press, 2003).
28. Jeong, I. K. et al. Direct observation of the formation of polar nanoregions in $PbMg_{1/3}Nb_{2/3}O_3$ using neutron pair distribution function analysis. *Phys. Rev. Lett.* **94**, 147602 (2005).
29. Zhang, N. et al. The missing boundary in the phase diagram of $PbZr_{1-x}Ti_xO_3$. *Nat. Commun.* **5**, 5231 (2014).
30. Senn, M. S., Keen, D. A., Lucas, T. C. A., Hriljac, J. A. & Goodwin, A. L. Emergence of long-range order in $BaTiO_3$ from local symmetry-breaking distortions. *Phys. Rev. Lett.* **116**, 207602 (2016).
31. Tucker, M. G., Keen, D. A., Dove, M. T., Goodwin, A. L. & Hui, Q. RMCProfile: reverse Monte Carlo for polycrystalline materials. *J. Phys. Condens. Matter* **19**, 335218 (2007).
32. Eremenko, M. et al. Local atomic order and hierarchical polar nanoregions in a classical relaxor ferroelectric. *Nat. Commun.* **10**, 2728 (2019).

33. Liu, H. et al. Emergence of high piezoelectricity from competing local polar order-disorder in relaxor ferroelectrics. *Nat. Commun.* **14**, 1007 (2023).
34. Dunmur, D. A., Fukuda, A. & Luckhurst, G. R. *Physical Properties of Liquid Crystals: Nematics* (London: IET Press, 2001).
35. Datta, K., Margaritescu, I., Keen, D. A. & Mihailova, B. Stochastic polarization instability in $PbTiO_3$. *Phys. Rev. Lett.* **121**, 137602 (2018).
36. Shirane, G. & Hoshino, S. On the phase transition in lead titanate. *J. Phys. Soc. Jpn.* **6**, 265–270 (1951).
37. Egerton, L. & Dillon, D. M. Piezoelectric and dielectric properties of ceramics in the system potassium-sodium niobate. *J. Am. Ceram. Soc.* **42**, 438–442 (1959).
38. Wang, X. et al. Giant piezoelectricity in potassium–sodium niobate lead-free ceramics. *J. Am. Chem. Soc.* **136**, 2905–2910 (2014).
39. Tao, H. et al. Ultrahigh performance in lead-free piezoceramics utilizing a relaxor slush polar state with multiphase coexistence. *J. Am. Chem. Soc.* **141**, 13987–13994 (2019).
40. Liu, Y. et al. Flexible polarization configuration in high-entropy piezoelectrics with high performance. *Acta Mater.* **236**, 118115 (2022).
41. Datta, K., Brajesh, K., Ranjan, R. & Mihailova, B. Adaptive dipolar correlation in ferroelectric $x(Ba_{0.7}Ca_{0.3})TiO_3$-$(1–x)Ba(Zr_{0.2}Ti_{0.8})O_3$. *Phys. Rev. B* **102**, 060102 (2020).
42. Cohen, R. E. Origin of ferroelectricity in perovskite oxides. *Nature* **358**, 136–138 (1992).
43. Heitmann, A. A. & Rossetti, G. A. Jr Thermodynamics of ferroelectric solid solutions with morphotropic phase boundaries. *J. Am. Ceram. Soc.* **97**, 1661–1685 (2014).
44. Luo, H. et al. Structural origin for the high piezoelectric performance of $(Na_{0.5}Bi_{0.5})TiO_3$-$BaTiO_3$-$BiAlO_3$ lead-free ceramics. *Acta Mater.* **218**, 117202 (2021).

Acknowledgements

This work was financially supported by Key Research and Development Program of Ministry of Science and Technology of China (No. 2022YFB3204000, J.C.), the Beijing Outstanding Young Scientist Program (JWZQ20240101015, J.C.), and the National Natural Science Foundation of China (Grant Nos. 22235002, J.C. and 22471013, H.L.). K.D. acknowledges the financial support from Deutsche Forschungsgemeinschaft (Heisenberg grant DA 2150/3-1). A portion of this research used resources at the Spallation Neutron Source, a DOE Office of Science User Facility operated by the Oak Ridge National Laboratory. The computational resource is provided by Westlake HPC Center.

Author contributions

J.C. and H.L. conceived this study. Y.Y. performed the experiments under the supervision of J.C. and H.L., and J.W. provided the KNN-based piezoelectric ceramic samples. K.D. and J.C.N. conduct the neutron total scattering measurements. Y.Y. and H.L. performed the Rietveld refinement of PDF and the RMC simulation. Y.Z. and M.G.T. checked and confirmed the process and results of RMC simulation. Y.Y. carried out the TEM and STEM analysis. S.L. and Y.H. performed the DFT calculations and analysis. Y.Y. wrote the first draft of the manuscript. H.L., J.C., K.D., and S.Z. revised the paper. All authors discussed the results and revised the manuscript.

Competing interests

The authors declare no competing interests.

Additional information

Supplementary information The online version contains supplementary material available at https://doi.org/10.1038/s41467-025-62701-1.

Correspondence and requests for materials should be addressed to Hui Liu or Jun Chen.

Peer review information *Nature Communications* thanks Zishen Tian, and the other, anonymous, reviewer(s) for their contribution to the peer review of this work. A peer review file is available.